Random Greedy Deployment of Heterogeneous UAVs

Yang Lv[1], Fengmin Wang[2], Xiankun Yu[1], Xin Li[3], Dachuan Xu[1], and Ruiqi Yang[1(✉)]

[1] Beijing Institute for Scientific and Engineering Computing, Beijing University of Technology, Beijing 100124, China
{lvyang,22062213}@emails.bjut.edu.cn, {xudc,yangruiqi}@bjut.edu.cn
[2] Jinghang Research Institute of Computing and Communication, Beijing 100074, China
[3] College of Economics and Management, Beijing University of Technology, Beijing 100124, China
lixinyz@bjut.edu.cn

Abstract. Unmanned Aerial Vehicles (UAVs) have been extensively utilized in environmental modeling tasks, including forest monitoring, agricultural mapping, and disaster assessment. These applications benefit from UAVs' ability to collect high-resolution data for purposes such as deforestation detection, crop management, and damage evaluation. However, the common assumption that UAVs are homogeneous leads to significant inaccuracies due to differences in UAV platforms and sensor characteristics. This paper investigates the deployment of heterogeneous UAVs equipped with various sensors in fire-affected regions, modeled via a point of interest framework. The goal is to minimize measurement errors by explicitly leveraging UAV heterogeneity. We introduce a weighted frame potential metric based on matrix orthogonality, and develop a randomized greedy algorithm to optimize UAV positioning. The proposed algorithm guarantees at least a 50% approximation of the optimal solution and offers a theoretical error bound on the metric. Experimental results demonstrate that the proposed method outperforms joint greedy and determinant-based algorithms in reducing measurement errors.

Keywords: UAV measurement · Approximation algorithm · Weighted frame potential · Submodular optimization

1 Introduction

UAVs are valuable tools for environmental management due to their mobility, adaptability, and sensor-carrying capabilities [20]. In environmental monitoring, UAV-mounted sensors are deployed to collect diverse data in various scenarios. However, key challenges remain, such as determining optimal UAV positions to improve detection accuracy.

M. Li et al. (Eds.): TAMC 2025, LNCS 16084, pp. 330–341, 2026.
https://doi.org/10.1007/978-981-95-4839-2_26

To better understand the deployment problem in UAV-based sensing, we first review related work in traditional sensor networks. In traditional sensor networks [1–17], sensors are typically considered homogeneous and independent, especially in linear observation models that solve linear inverse problems for reconstructing physical fields. A substantial amount of research focuses on selecting k points from N candidate locations to maximize information gain and minimize errors. This forms a combinatorial optimization problem, which has led to the development of numerous heuristic and approximation algorithms. Most studies aim to design various metrics to assess and minimize computational error, and then develop optimization algorithms that exploit the properties of these metrics. While significant progress is made in coupling metrics with algorithms [3], research on heterogeneous UAV measurements remains limited, with most studies addressing homogeneous sensor issues. UAV heterogeneity stems from differences in sensor models, often caused by variations in procurement timing or manufacturing inconsistencies. These variations lead to distinct sensor errors, and treating all UAVs as homogeneous results in a model that poorly reflects real-world conditions. Effectively coordinating these heterogeneous UAVs for accurate detection remains a challenging task [21].

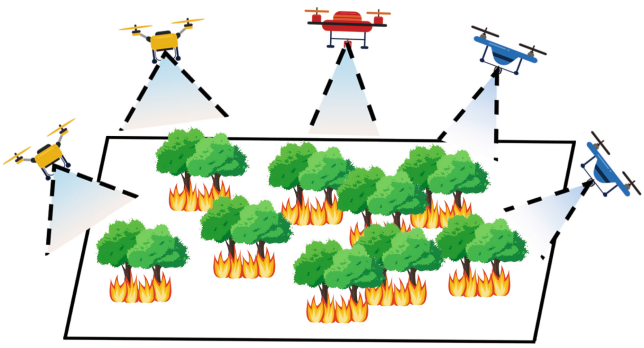

Fig. 1. Heterogeneous UAV Measurement Challenge: This study addresses a scenario involving multiple distinct UAV types. In the figure, the fleet consists of two yellow UAVs, two blue UAVs and one red UAV, each type exhibiting different accuracy levels. The objective is to ascertain the optimal deployment of these UAVs to reduce detection errors as much as possible in monitoring forest fires. (Color figure online)

We investigate how UAVs equipped with sensors of varying accuracies can collaboratively measure fire-affected areas and reconstruct the fire scene to identify hazardous zones. This approach is also applicable to real-time forest fire warnings. We assume a set of predefined points of interest, where UAVs hover to collect measurements. The collected data is transmitted to a central system, which reconstructs the overall fire scenario, as illustrated in Fig. 1. Each UAV group is subject to Gaussian noise with a distinct variance. The goal is to determine an optimal UAV deployment strategy that solves a linear inverse problem

while minimizing reconstruction error. Due to the challenges introduced by sensor heterogeneity, new metrics are needed. Classical criteria such as mutual information or A-optimality fail to explicitly capture sensor heterogeneity. To address this issue, we propose the *weighted frame potential (WFP)*, which fully accounts for the accuracy differences among heterogeneous sensors. The proposed metric is submodular, enabling the use of a random greedy algorithm. The submodularity of WFP ensures that the random greedy algorithm can provide provable approximation guarantees for this otherwise intractable selection problem, while maintaining high computational efficiency.

The main contributions of this paper are summarized as follows:

- We address the problem of environmental modeling using heterogeneous UAVs, particularly in scenarios involving multiple UAV groups.
- Despite differences in UAV models and factory configurations, we show that effective collaborative detection can still be achieved.
- We introduce the weighted frame potential metric and apply a random greedy algorithm, which guarantees a solution that is at least $1/2$ of the optimal. Our method provides a provable performance bound.
- We further provide an upper bound on the solution quality based on the weighted frame potential.

2 Problem Statement

2.1 UAVs Model

A forest fire has occurred, requiring heterogeneous UAVs to investigate the affected area. The fire is assumed to be located on a two-dimensional plane. On this plane, there are N candidate locations that require observation, denoted by the set $\mathcal{N} = \{1, 2, \ldots, N\}$. Each candidate point is more suitable for specific types of UAVs. Thus, the set $\mathcal{N}$ can be partitioned into subsets $S_1, S_2, \ldots, S_m \subseteq \mathcal{N}$, where S_i represents the points assigned to UAVs of type i, for $i = 1, 2, \ldots, m$. The objective is to select appropriate locations from the candidate set to deploy the UAVs, such that the estimation of the fire scene is as accurate as possible.

Since the number of UAVs available for each type is fixed, any feasible deployment $\mathcal{L} \subseteq \mathcal{N}$ must satisfy the UAV-type constraints. Specifically, if M_i UAVs of type i are available, then the solution must satisfy $|\mathcal{L} \cap S_i| = M_i$. The total number of deployed UAVs is given by $|\mathcal{L}| = \sum_{i=1}^{m} M_i$. In other words, all UAVs must be assigned to their designated subsets, and their total usage matches the available inventory.

2.2 UAVs Placement Problem

Suppose the goal is to reconstruct the temperature at K selected points. The corresponding true values are denoted by $\boldsymbol{\alpha} \in \mathbb{R}^K$. At each PoI, the temperatures at the K detection points will influence the measurement at this PoI. In addition,

each PoI measurement is corrupted by Gaussian noise associated with the UAV's sensor. Following the sensing model in [9], the aggregated measurements across all candidate points can be expressed as

$$\boldsymbol{f} = \boldsymbol{\Psi}\boldsymbol{\alpha} + \boldsymbol{\eta}, \tag{1}$$

The differences in each row of $\boldsymbol{\Psi} \in \mathcal{R}^{N\times K}$ reflect variations in the spatial distribution of UAVs, where more similar vectors indicate closer distances. The differences in each row of $\boldsymbol{\Psi}$ reflect variations in the spatial distribution of UAVs. $\boldsymbol{\eta}$ represents additive measurement noise. The errors across all UAVs stem from an N-dimensional vector $\boldsymbol{\eta} \in \mathbb{R}^N$, where $\boldsymbol{\eta}$ is additive zero-mean white measurement noise with a variance matrix $\boldsymbol{C}$.

The covariance matrix $\boldsymbol{C}$ is a diagonal matrix $\boldsymbol{C} = \mathbf{diag}(\sigma_1^2, \sigma_2^2, ..., \sigma_N^2)$, where UAVs of the same type have the same variance. Furthermore, outstanding UAVs are characterized by smaller variances. For all UAVs belonging to the j-th type, σ_i^2 remains consistent for any $i \in S_j$.

If the set of observation positions $\mathcal{L}$ for the UAV is determined, the vector obtained from the measurements is denoted by $\boldsymbol{f}_{\mathcal{L}} \in \mathbb{R}^{|\mathcal{L}|}$, where $\boldsymbol{f}_{\mathcal{L}}$ represents the sub-vector of $\boldsymbol{f}$ indexed by $\mathcal{L}$. Simultaneously, $\boldsymbol{\eta}_{\mathcal{L}}$ signifies the sub-vector of $\boldsymbol{\eta}$ indexed by $\mathcal{L}$. $\boldsymbol{\Psi}_{\mathcal{L}} \in \mathbb{R}^{|\mathcal{L}|\times K}$ corresponds to the sub-matrix of $\boldsymbol{\Psi}$, formed by the rows indexed by $\mathcal{L}$. The resultant sub-formula from observations is given by:

$$\boldsymbol{f}_{\mathcal{L}} = \boldsymbol{\Psi}_{\mathcal{L}}\boldsymbol{\alpha} + \boldsymbol{\eta}_{\mathcal{L}} \tag{2}$$

Because the number of UAVs is limited and cannot cover all selected points, the size of the measurement results from $\boldsymbol{f}_{\mathcal{L}}$ is smaller than that of $\boldsymbol{f}$. This reduction in scale decreases the precision in describing the physical scene $\boldsymbol{\alpha}$. Therefore, the central challenge of this paper is to effectively utilize the limited heterogeneous UAVs to enhance the description of $\boldsymbol{\alpha}$.

2.3 Weighted Frame Potential (WFP)

Reconstructing the temperature typically requires different criteria to evaluate the effectiveness of the references. Previous works have proposed various criteria such as MSE [22], VCE [13], and WCEV [14] to assess performance. Benedetto et al. [15] introduce an approach centered around the concept of frame potential. Building on this foundation, subsequent research extended the frame potential metric to incorporate heterogeneous metrics, leading to the development of the weighted frame potential. Let the chosen set be denoted as $\mathcal{L}$. Define $\boldsymbol{\Psi}_{\mathcal{L}} = \{\boldsymbol{\psi}_1, \boldsymbol{\psi}_2, \ldots, \boldsymbol{\psi}_L\}$, where $\boldsymbol{\psi}_i$ represents the i-th row vector of $\boldsymbol{\psi}_{\mathcal{L}}$. The weighting coefficients are given by $\omega_i = \sigma_i$.

$$WFP(\boldsymbol{\Psi}_{\mathcal{L}}) = \sum_{i,j\in\mathcal{L}} \omega_i\omega_j \frac{\langle \boldsymbol{\psi}_i, \boldsymbol{\psi}_j \rangle^2}{\|\boldsymbol{\psi}_i\|_2^2 \cdot \|\boldsymbol{\psi}_j\|_2^2}. \tag{3}$$

Since the primary objective is to minimize the weighted frame potential, it becomes evident that larger variances in UAV measurement errors lead to

poorer evaluations of the WFP's performance metric, so the logical strategy is to increase the corresponding ω values. Research [6] findings indicate that in scenarios involving two groups of UAVs, $\omega_i = \frac{1}{1+\exp(-(\sigma_i-\overline{\sigma}))}$ performs better, wherein $\overline{\sigma}$ symbolizes the average error across UAVs. In scenarios involving multiple groups of UAVs, this paper discovers that setting $\omega_i = \sigma_i$ leads to favorable performance. In other words, selecting ω_i as the standard deviation corresponding to index i yields superior results.

Minimizing the WFP presents significant challenges in algorithm design. To address this, a monotone, normalized, and submodular function f is constructed. The core principle behind constructing f is to identify the complement of the solution set and exclude row vectors that minimally decrease the value of WFP. These positions are deemed unsuitable for UAV placement. Through this construction, the function f becomes

$$f(\mathcal{L}) = WFP(\boldsymbol{\Psi}_{\mathcal{N}}) - WFP(\boldsymbol{\Psi}_{\mathcal{N}\setminus\mathcal{L}}). \tag{4}$$

We start by proving the normalization of function f. When $\mathcal{L} = \emptyset$, the following holds:

$$\begin{aligned} f(\mathcal{L}) &= WFP(\boldsymbol{\Psi}_{\mathcal{N}}) - WFP(\boldsymbol{\Psi}_{\mathcal{N}\setminus\emptyset}) \\ &= WFP(\boldsymbol{\Psi}_{\mathcal{N}}) - WFP(\boldsymbol{\Psi}_{\mathcal{N}}) \\ &= 0. \end{aligned} \tag{5}$$

This confirms that when the set $\mathcal{L}$ is empty, $f(\mathcal{L})$ evaluates to 0, thereby satisfying the normalization property.

Based on the definition of WFP in Equation (3), observing that the summation terms of WFP are positive and the number of terms increases as $\mathcal{L}$ grows, it can be deduced that WFP is a monotonically increasing function. Therefore, the complement of the set denoted as $WFP(\boldsymbol{\Psi}_{\mathcal{N}\setminus\mathcal{L}})$, is a monotonically decreasing function. Consequently, the expression $WFP(\boldsymbol{\Psi}_{\mathcal{N}}) - WFP(\boldsymbol{\Psi}_{\mathcal{N}\setminus\mathcal{L}})$ represents a monotonically increasing function.

Next, we establish the submodularity property for any two sets, $\mathcal{L}_1$ and $\mathcal{L}_2$, within $\mathcal{N}$, where $\mathcal{L}_1 \subseteq \mathcal{L}_2 \subseteq \mathcal{N}$. For any element $e \notin \mathcal{L}_2$, we aim to prove the submodularity condition.

$$\begin{aligned} &f(\mathcal{L}_1 \cup \{e\}) - f(\mathcal{L}_1) \\ &= \big(WFP(\boldsymbol{\Psi}_{\mathcal{N}}) - WFP(\boldsymbol{\Psi}_{\mathcal{N}\setminus(\mathcal{L}_1\cup\{e\})})\big) - \big(WFP(\boldsymbol{\Psi}_{\mathcal{N}}) - WFP(\boldsymbol{\Psi}_{\mathcal{N}\setminus\mathcal{L}_1})\big) \\ &= WFP(\boldsymbol{\Psi}_{\mathcal{N}\setminus\mathcal{L}_1}) - WFP(\boldsymbol{\Psi}_{\mathcal{N}\setminus(\mathcal{L}_1\cup\{e\})}) \\ &= \sum_{i\in\mathcal{N}\setminus(\mathcal{L}_1\cup\{e\})} \omega_i\omega_e \frac{\langle \boldsymbol{\psi}_i, \boldsymbol{\psi}_e\rangle^2}{\|\boldsymbol{\psi}_i\|_2^2 \cdot \|\boldsymbol{\psi}_e\|_2^2} \\ &\quad + \sum_{j\in\mathcal{N}\setminus(\mathcal{L}_1\cup\{e\})} \omega_e\omega_j \frac{\langle \boldsymbol{\psi}_e, \boldsymbol{\psi}_j\rangle^2}{\|\boldsymbol{\psi}_e\|_2^2 \cdot \|\boldsymbol{\psi}_j\|_2^2} + \omega_e\omega_e \frac{\langle \boldsymbol{\psi}_e, \boldsymbol{\psi}_e\rangle^2}{\|\boldsymbol{\psi}_e\|_2^2 \cdot \|\boldsymbol{\psi}_e\|_2^2} \end{aligned} \tag{6}$$

Since $\mathcal{L}_1$ is contained within $\mathcal{L}_2$, the number of terms in the given expression reduces. We can establish the submodularity property by demonstrating that: $f(\mathcal{L}_1 \cup \{e\}) - f(\mathcal{L}_1) \geq f(\mathcal{L}_2 \cup \{e\}) - f(\mathcal{L}_2)$.

By taking these steps, we have demonstrated that f is normalized, monotone, and submodular. Based on these properties, we can present an approximation algorithm for f.

3 Algorithm and Theoretical Foundation

In this section, the heterogeneous UAV placement problem is tackled by solving a submodular maximization problem. The algorithm employed here is the random greedy algorithm, which offers a straightforward way to demonstrate the theoretical guarantees of this approach.

3.1 Algorithm

f is a normalized, monotone submodular function. Given that the number of UAV of the i-th model is denoted as M_i, the constraints of the problem can be expressed as $|(\mathcal{N} \setminus \mathcal{L}) \cap S_i| = M_i$. Assuming $|S_i|$ represents the number of elements in S_i, the problem can be simplified as $|\mathcal{L} \cap S_i| = |S_i| - M_i$, where let us denote $M_i' = |S_i| - M_i$, $L' = \sum_{i=1}^{m} M_i'$ for simplicity. This can be framed as an optimization problem:

$$\begin{aligned} &\arg\max_{\mathcal{L} \subseteq \mathcal{N}} f(\mathcal{L}), \\ &s.t. |\mathcal{L} \cap S_i| = M_i' \quad \text{for } i \text{ from 1 to } m \end{aligned} \tag{7}$$

For such a problem, when $m = 1$, it becomes a classic submodular function maximization problem [19]. Utilizing a greedy algorithm, the problem can be solved to yield a value of the f function that is $1 - 1/e$ times the optimal solution. Next, the aim is to extend this algorithm to the scenario where m is an arbitrary constant.

Algorithm 1 The random greedy algorithm for submodular maximization problems

Require: submodular function $f : 2^{\mathcal{N}} \rightarrow \mathbb{R}$, ground set $S_1, S_2, ..., S_m$, restrictions $M_1', M_2', ..., M_m'$

1: Create a multi-element index list T containing M_1' instances of 1, M_2' instances of 2, ..., M_m' instances of m. {This list is used to determine the order of sensor placement in a greedy manner.}
2: Randomly permute this list
3: **for** each element j in the list, taken from the head of the list **do**
4: $v_i = \arg\max_{v_i \in S_j} f(T \cup \{v_i\}) - f(T)$
5: $T \leftarrow T \cup \{v_i\}$
6: **end for**
7: return T

A greedy algorithm is employed to address this issue. Although the subsequent approximation ratio analysis applies to all greedy algorithms, numerical

experiments have shown that the random greedy algorithm yields the best performance. Therefore, we only introduce the random greedy algorithm here. The algorithm first randomly shuffles the selection order of M_1' elements from S_1, M_2' elements from S_2, and so on before execution. Each time, the UAV is placed at the position with the highest marginal gain among the corresponding elements.

3.2 Algorithm Approximation Guarantee

Given that f is a submodular function, the marginal gain of set A over set B according to the function f is defined as $f(A|B) = f(A \cup B) - f(B)$. If A is an element rather than a set, then $f(A|B) = f(A \cup B) - f(B)$. Let us establish the proof that for any chosen subset $V \subseteq \mathcal{N}$, the function $f(\cdot|V)$ exhibits submodularity.

$$\begin{aligned} & f(A|V) + f(B|V) \\ =& f(A \cup V) - f(V) + f(B \cup V) - f(V) \\ =& (f(A \cup V) + f(B \cup V)) - 2f(V) \\ \geq& f(A \cup B \cup V) + f((A \cap B) \cup V) - 2f(V) \\ =& f(A \cup B|V) + f(A \cap B|V) \end{aligned} \tag{8}$$

The inequality is based on the properties of the submodular function of f.

We define the optimal solution of the submodular function as OPT and introduces the definitions $OPT_1 = OPT \cap S_1$, $OPT_2 = OPT \cap S_2$, ..., $OPT_m = OPT \cap S_m$. Here, OPT_i represents the elements within S_i that are part of the optimal solution OPT. Let T_i denote the outcome of set T after completing the i-th round of iterations. Given that OPT is a valid set of solutions, we have $|OPT_i| = M_i'$ for all i from 1 to m.

We establish a collection of bijections from $T \cap S_j$ to OPT_j. If an element $e_j \in (T \cap S_j) \cap OPT_j$, we map e_j to itself. The remaining elements from $T \cap S_j$ lie in $(T \cap S_j) \setminus OPT_j$, and we randomly construct a bijection from $(T \cap S_j) \setminus OPT_j$ to $OPT_j \setminus (T \cap S_j)$. This way, a mapping is established from $v_i \in T \cap S_j$ to $o_i^j \in OPT_j$. Next, we show that $f(v_i|S_{i-1}) \geq f(o_i^j|S_{i-1})$. If v_i is in the set $(T \cap S_j) \cap OPT_j$, it is evident that v_i and o_i^j are the same element. T_0 is defined as the empty set. If v_i lies in the set $(T \cap S_j) \setminus OPT_j$, and in the i-th round of greedy selection, v_i is chosen while o_i^j is not, it implies $f(v_i|T_{i-1}) \geq f(o_i^j|T_{i-1})$.

Based on the above discussion, this inequality holds.

$$\begin{aligned} f(T) &= \sum_{j=1}^{m} \sum_{i \in A_j} f(v_i|T_{i-1}) \\ &\geq \sum_{j=1}^{m} \sum_{i \in A_j} f(o_i^j|T_{i-1}) \geq \sum_{j=1}^{m} \sum_{i \in A_j} f(o_i^j|T) \\ &\geq \sum_{j=1}^{m} f(OPT_j|T) \geq f\left(\bigcup_{j=1}^{m} OPT_j|T\right) \\ &= f(OPT|T) \geq f(OPT) - f(T) \end{aligned} \tag{9}$$

The first inequality follows from the constructed bijections mentioned earlier. The second inequality is a consequence of the submodularity of f and the fact that $T_{i-1} \subseteq T$. The third and fourth inequalities stem from the submodularity of $f(\cdot|T)$. The fifth inequality holds due to the monotonicity property of f, where $OPT \subseteq (OPT \cup T)$. By simplifying (9), we arrive at the result $f(T) \geq \frac{1}{2} f(OPT)$.

Theorem 1. *For any heterogeneous UAV placement problem, assuming* $\overline{OPT} = \arg\min_{\mathcal{A} \subseteq \mathcal{N}, |\mathcal{A} \cap S_i| = M_i} WFP(\mathcal{A})$*, and considering the sub-optimal solution found using the greedy algorithm as* $\mathcal{N} \setminus T$*, the relationship between* $\boldsymbol{\Psi}_{\mathcal{N} \setminus T}$ *and* $\boldsymbol{\Psi}_{\overline{OPT}}$ *is as follows:*

$$WFP(\boldsymbol{\Psi}_{\mathcal{N} \setminus T}) \leq \gamma WFP(\boldsymbol{\Psi}_{\overline{OPT}}) \tag{10}$$

where $\gamma = \frac{1}{2}\left(1 + WFP(\boldsymbol{\Psi}) \frac{K}{L_{min}^2}\right)$ *is the approximation factor and* $L_{min} = \min_{|\mathcal{L}|=L} \sum_{i \in L} \sigma_i^2 \left\|\boldsymbol{\psi}_i\right\|^2$.

Proof. The detailed proof of this result is omitted here for brevity and will be included in an extended version.

This establishes the theoretical guarantee for the upper bound of the approximation algorithm's performance measured by the WFP metric. As the values of the WFP in $\boldsymbol{\Psi}_{\mathcal{N} \setminus \mathcal{L}}$ decrease, $\boldsymbol{\Psi}_{\mathcal{N} \setminus \mathcal{L}}$ approaches orthogonality, resulting in a smaller error.

4 Numerical Results

In this section, we analyze the performance of the algorithm proposed in the paper and compare it with algorithms from other studies through numerical experiments. This section focuses on a large-scale scenario to test the algorithms.

We compare our random greedy algorithm with three other algorithms as follows:

Random Greedy Algorithm (RGA): The WFP and random greedy algorithm are utilized to select points where UAVs cannot be placed, and then their complements are determined. The random greedy algorithm randomly selects a category at each step and removes an element from it. The final result must precisely satisfy the specified constraints.

Joint Greedy Algorithm (JGA) [6]**:** The algorithm identifies the largest potential point from all available potential points that do not exceed the constraints and then determines its complement for UAV placement. Similarly, it shares the same theoretical upper bound as RGA.

medskip**Determinant Algorithm (DA)** [11]**:** The calculation of UAVs with different accuracies is conducted in stages. In each step of the process, the algorithm identifies the value of j corresponding to the maximum marginal gain, which is given by $\log\det\left(\overline{\sigma}^{-2}\sum_{i\in S}\boldsymbol{\psi}_i\tilde{\boldsymbol{\psi}}_i+\boldsymbol{\psi}_j\tilde{\boldsymbol{\psi}}_j+\boldsymbol{\Sigma}^{-1}\right)$. This algorithm is solely dependent on $\overline{\sigma}$ and does not take into account the heterogeneity among UAVs.

Random Algorithm (RA): Potential points that meet the problem requirements are selected from each category of UAV locations for UAV placement.

In large-scale fires, dispatching UAVs for disaster site observation is of utmost importance. The selected area for fire observation is 1km × 2km, with the average temperature ranging from 30 to 400 °C. The fire data are obtained via interpolation of regression models based on a set of points. From Fig. 2, the distribution of the fire is quite distinct, with two prominent high-temperature regions. The algorithm should strive to depict these two hotspots as accurately as possible.

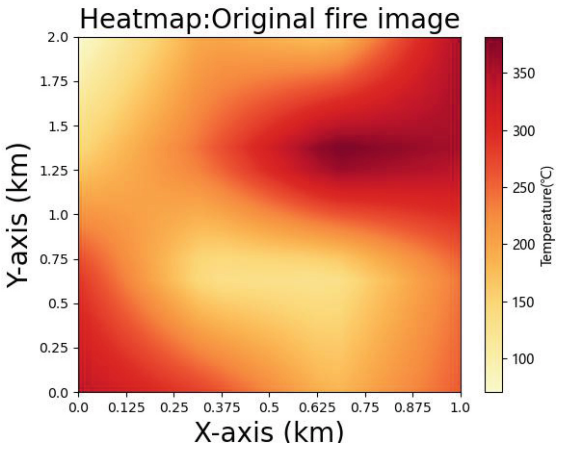

Fig. 2. A simulated fire scene heatmap measuring 2km × 1km.

In this scenario, two types of UAVs are deployed: one type comprises 20 UAVs with 80 potential locations, and the other type consists of 55 UAVs with 200

potential locations. The UAVs have variance values of 2 and 6 respectively. To reconstruct the fire disaster scene, the UAVs primarily observe the temperatures at 75 specific points on the fire site. The overall fire disaster scene is approximated using interpolation techniques. The matrix $\boldsymbol{\Psi}$ is designed as a 280×75 matrix, which serves as a sub-matrix of a 280-dimensional orthogonal matrix. For the algorithmic approach, only the RGA, JGA, DA and RA from this study are considered.

The algorithmic results reveal that the execution times for RGA, JGA, DA, and RA are 0.007 s, 0.007 s, 34.6 s, and 0.0 s, respectively. It is noticeable that RGA and JGA continue to maintain a rapid execution speed, while DA experiences a sharp increase in runtime due to the high time complexity associated with determinant calculations. Therefore, DA is not a favorable choice for large-scale scenarios, as its performance significantly degrades in such cases.

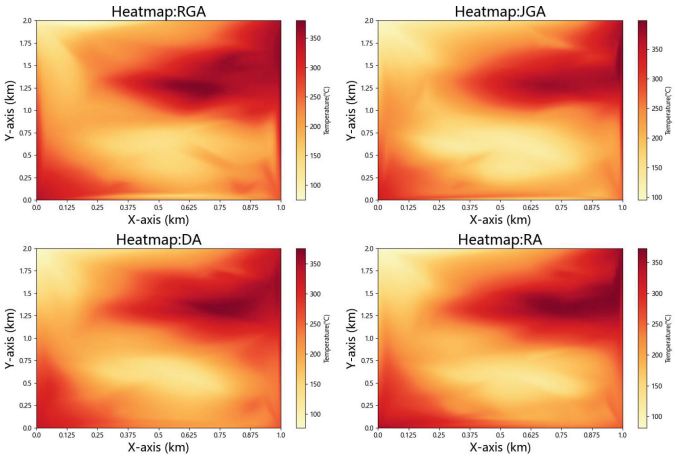

Fig. 3. Interpolated fire scene plots provided by the four algorithms: top-left for RGA, top-right for JGA, bottom-left for DA, and bottom-right for RA.

The measurement results of the algorithms are fitted using interpolation to obtain Fig. 3. Intuitively, it is evident that the fitting outcome of the RGA image in the top-left corner is the most favorable, clearly displaying the two hotspots on the image while achieving excellent results for other intermediate areas. The poor fitting performance of the other images can be attributed to inaccurate measurement results, which negatively impact the quality of the fit. Specific numerical values, as depicted in Fig. 4, reveal that RGA performs the best in terms of both MSE and average temperature difference in larger-scale data scenarios. The average temperature difference is improved by 4.0% compared to the DA algorithm. These numerical results align with the patterns observed in the previous images. Thus, RGA proves to be a fast and accurate algorithm in larger-scale scenarios.

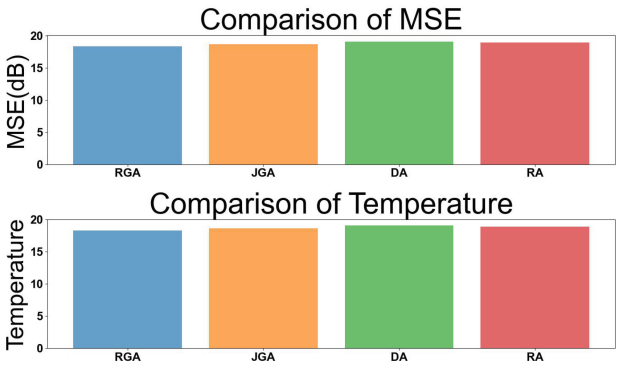

Fig. 4. Comparison chart of MSE and average temperature difference among the four algorithms in the large-scale fire detection scenarios.

5 Conclusion

This paper studies a measurement problem with multiple groups of heterogeneous UAVs. Each group has a limited number of UAVs. The goal is to reduce errors in solving linear inverse problems. A submodular maximization algorithm is proposed using the weighted frame potential. Its upper bound is rigorously proven. The algorithm is tested in large-scale fire scenarios. The results indicate that it outperforms other methods in terms of speed. Additionally, it reduces the average errors by 4.0% in large-scale fire observations. Future research could further explore the combination of UAV placement and dynamic target tracking [18] for improved disaster monitoring.

Acknowledgement. This work was partially supported by Beijing Natural Science Foundation (Nos. Z220004, IS24001, QY24081).

References

1. Ranieri, J., Chebira, A., Vetterli, M.: Near-optimal sensor placement for linear inverse problems. IEEE Trans. Signal Process. **62**(5), 1135–1146 (2014)
2. Bian, F., Kempe, D., Govindan, R.: Utility based sensor selection. In: Proceedings of the 5th International Conference on Information Processing in Sensor Networks, pp. 11–18. ACM, Nashville (2006)
3. Li, B., Liu, H., Wang, R.: Efficient sensor placement for signal reconstruction based on recursive methods. IEEE Trans. Signal Process. **69**, 1885–1898 (2021)
4. Zhou, H., Li, X., Cher, C.Y., Kursun, E., Qian, H., Yao, S.C.: An information-theoretic framework for optimal temperature sensor allocation and full-chip thermal monitoring. In: Proceedings of the 49th Annual Design Automation Conference, pp. 642–647. ACM, San Francisco (2012)
5. Rusu, C., Thompson, J., Robertson, N.M.: Sensor scheduling with time, energy, and communication constraints. IEEE Trans. Signal Process. **66**(2), 528–539 (2017)

6. Majumder, K., Pillai, S. B., Mulleti, S.: Greedy Selection for Heterogeneous Sensors. arXiv preprint arXiv:2307.00840 (2023)
7. Welch, W.J.: Branch-and-bound search for experimental designs based on D optimality and other criteria. Technometrics **24**(1), 41–48 (1982)
8. Krause, A., Singh, A., Guestrin, C.: Near-optimal sensor placements in Gaussian processes: theory, efficient algorithms and empirical studies. J. Mach. Learn. Res. **9**(2), 235–284 (2008)
9. Jamali-Rad, H., Simonetto, A., Leus, G.: Sparsity-aware sensor selection: centralized and distributed algorithms. IEEE Signal Process. Lett. **21**(2), 217–220 (2014)
10. Liu, S., Vempaty, A., Fardad, M., Masazade, E., Varshney, P.K.: Energy-aware sensor selection in field reconstruction. IEEE Signal Process. Lett. **21**(12), 1476–1480 (2014)
11. Joshi, S., Boyd, S.: Sensor selection via convex optimization. IEEE Trans. Signal Process. **57**(2), 451–462 (2008)
12. Chepuri, S.P., Leus, G.: Sparsity-promoting sensor selection for non-linear measurement models. IEEE Trans. Signal Process. **63**(3), 684–698 (2014)
13. Shamaiah, M., Banerjee, S., Vikalo, H.: Greedy sensor selection: leveraging submodularity. In: 49th IEEE Conference on Decision and Control, pp. 2572–2577. IEEE, Atlanta (2010)
14. Jiang, C., Soh, Y.C., Li, H.: Sensor placement by maximal projection on minimum eigenspace for linear inverse problems. IEEE Trans. Signal Process. **64**(21), 5595–5610 (2016)
15. Benedetto, J.J., Fickus, M.: Finite normalized tight frames. Adv. Comput. Math. **18**, 357–385 (2003)
16. Alonso, A.A., Kevrekidis, I.G., Banga, J.R., Frouzakis, C.E.: Optimal sensor location and reduced order observer design for distributed process systems. Comput. Chem. Eng. **28**(1–2), 27–35 (2004)
17. Mokhasi, P., Rempfer, D.: Optimized sensor placement for urban flow measurement. Phys. Fluids **16**(5), 1758–1764 (2004)
18. Lv, Y., Fan, G., Li, M., Liu, X., Liu, P., Zhang, Y.: UAV target tracking with bandit-based data fusion. In: International Conference on Combinatorial Optimization and Applications, Beijing, China, pp. 278–286 (2024)
19. Nemhauser, G.L., Wolsey, L.A., Fisher, M.L.: An analysis of approximations for maximizing submodular set functions—I. Math. Program. **14**, 265–294 (1978)
20. Fang, Z., Savkin, A.V.: Strategies for optimized UAV surveillance in various tasks and scenarios: a review. Drones **8**(5), 1–41 (2024)
21. Sultan, L., Anjum, M., Rehman, M., Murawwat, S., Kosar, H.: Communication among heterogeneous unmanned aerial vehicles (UAVs): classification, trends, and analysis. IEEE Access **9**, 118815–118836 (2021)
22. Jiang, C., Chen, Z., Su, R., Soh, Y.C.: Group greedy method for sensor placement. IEEE Trans. Signal Process. **67**(9), 2249–2262 (2019)